JOURNAL OF GUIDANCE, CONTROL, AND DYNAMICS
Vol. 24, No. 2, March–April 2001

Multiresolution Methods for Reduced-Order Models for Dynamical Systems

Andrew J. Kurdila* and Richard J. Prazenica†
University of Florida, Gainesville, Florida 32611-6250
and
Othon Rediniotis‡ and Thomas Strganac§
Texas A&M University, College Station, Texas 77843-3141

Reduced-order input/output models are derived for a class of nonlinear systems by utilizing wavelet approximations of kernels appearing in Volterra series representations. Although Volterra series representations of nonlinear system input/output have been understood from a theoretical standpoint for some time, their practical use has been limited as a result of the dimensionality of approximations of the higher-order, nonlinear terms. In general, wavelets and multiresolution analysis have shown considerable promise for the compression of signals, images, and, most importantly here, some integral operators. Unfortunately, causal Volterra series representations are expressed in terms of integrals that are restricted to products of half-spaces, and there is a significant difficulty in deriving wavelets that are appropriate for Volterra kernel representations that are restricted to semi-infinite domains. In addition, it is necessary to derive Volterra kernel expansions that are consistent with the method of sampling used to obtain the input and output data. This paper derives discrete approximations for truncated Volterra series representations in terms of a specific class of biorthogonal wavelets. When a zero-order hold is used for both the input and output signals, it is shown that a consistent approximation of the input/output system is achieved for a specific choice of biorthogonal wavelet families. This family is characterized by the fact that all of the wavelets are biorthogonal with respect to the characteristic function of the dyadic intervals used to define the zero-order hold. It is also simple to show that an arbitrary choice of wavelet systems will not, in general, provide a consistent approximation for arbitrary input/output mappings. Numerical studies of the derived methodologies are carried out by using experimental pitch/plunge response data from the TAMU Nonlinear Aeroelastic Testbed.

Nomenclature

$\{a_k\}$	=	primary scaling function filters
$\{\tilde{a}_k\}$	=	dual scaling function filters
$\{b_k\}$	=	primary wavelet filters
$\{\tilde{b}_k\}$	=	dual wavelet filters
$h_{1,j,m}$	=	discrete first-order Volterra kernel
$h_1(\xi)$	=	first-order Volterra kernel
$h_{2,j,(r,s)}$	=	discrete second-order Volterra kernel
$h_2(\xi, \eta)$	=	second-order Volterra kernel
j	=	dilation index
k, m, p, r, s	=	translation indices
n	=	sampling index
t	=	time
$u(t)$	=	system input
$y(t)$	=	system output
$y_i(t)$	=	output of the ith-order Volterra operator
$y_{1,j,n}$	=	discrete output of the first-order Volterra operator
$y_{2,j,(r,s)}$	=	discrete output of the second-order Volterra operator
$\{\alpha_{j,k}\}$	=	one-dimensional scaling function coefficients
$\{\alpha_{j,(r,s)}\}$	=	two-dimensional scaling function coefficients
$\{\beta_{j,k}\}$	=	one-dimensional wavelet coefficients
$\{\beta^1_{j,(r,s)}\}, \{\beta^2_{j,(r,s)}\}, \{\beta^3_{j,(r,s)}\}$	=	two-dimensional wavelet coefficients
$\Phi(x, y)$	=	two-dimensional tensor product scaling function
$\phi(x)$	=	primary scaling function
$\tilde{\phi}(x)$	=	dual scaling function
$\chi(t)$	=	characteristic function
$\psi(x)$	=	primary wavelet
$\tilde{\psi}(x)$	=	dual wavelet
$\psi^1(x, y), \psi^2(x, y), \psi^3(x, y)$	=	two-dimensional tensor product wavelets

Received 13 September 1999; revision received 18 June 2000; accepted for publication 5 July 2000.

*Associate Professor, Department of Aerospace Engineering, Mechanics and Engineering Science.
†Graduate Research Assistant, Department of Aerospace Engineering, Mechanics and Engineering Science.
‡Assistant Professor, Department of Aerospace Engineering.
§Associate Professor, Department of Aerospace Engineering.

I. Introduction

A LARGE collection of methods have been investigated for obtaining reduced-order representations of linear and nonlinear dynamical systems in structural mechanics, fluid mechanics, aeroelasticity, and control theory. These methods include such diverse strategies as modal synthesis, Ritz vector reduction, rational approximation, Hankel approximation, and proper orthogonal decomposition (POD). In fluid mechanics, the study of the qualitative dynamics of various classes of flows using POD has been carried out in Refs. 1 and 2. In these studies, the essential goal is often to study the topological dynamics underlying the more complex model.[1–3] Sometimes, the ultimate goal is the development of control experiments or methodologies.[4] In structural mechanics, Ritz basis reduction methods denoted "component mode synthesis" have emerged as a distinct discipline (see Ref. 5). Order reduction methods designed to improve the fidelity of specific measurements, observations, or performance functionals have been studied in linear control theory (see Ref. 6). Similarly, some researchers have used reduced basis methods in the simulation and control of the nonlinear Navier–Stokes equations.[7–9] More recently, component mode synthesis methods have been studied for a class of open-loop simulations of aeroelastic systems.[10–12]

Despite the considerable collection of research for achieving low-order model approximations in diverse fields, there remain significant barriers to the realization of general reduced-order representations specifically for the control of nonlinear systems. We seek to address one limitation of most of the order reduction methods

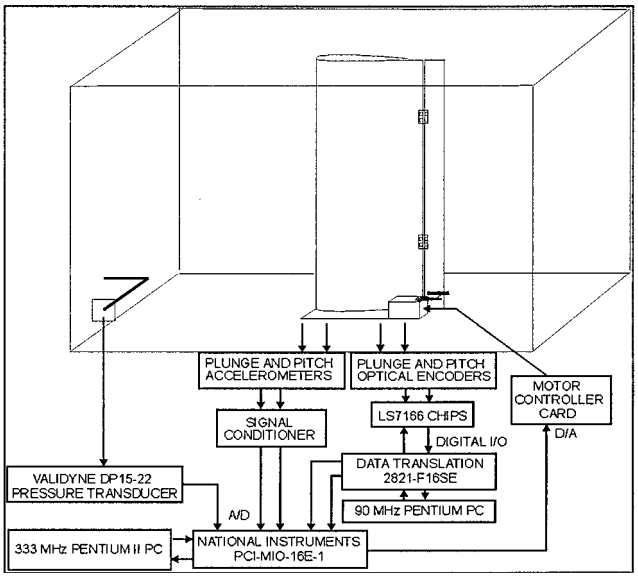

Fig. 1 Prototypical nonlinear aeroelastic system (D/A, digital to analog; I/O, input/output).

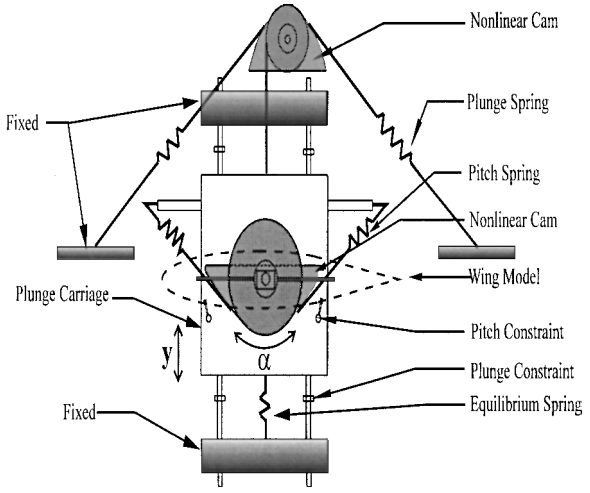

Fig. 2 Carriage design.

listed above. One common feature of most of these methods is that they are not directly amenable to online updating or adaptive subspace selection strategies. The approach taken in this paper builds on, and in some sense stands in contrast to, recent research by the authors in nonlinear aeroelasticity and nonlinear control. The authors have shown that geometrically nonlinear control methods can be extremely effective in some applications to nonlinear aeroelastic control.[10–12] Fundamentally, these strategies rely on an accurate reduced-order model of the nonlinear open-loop dynamics. These control strategies have been tested and verified on the same experimental apparatus that is shown in Figs. 1 and 2. At the same time, the authors have shown that some POD reduced basis methods can be extremely effective in generating low-dimensional approximations of uncontrolled flow. As an example, the authors have studied the efficiency of POD methods for obtaining reduced-order models of synthetic jets.[4] The performance of this approach for studying a particular response regime is discussed in detail in Ref. 4.

It would seem natural, and appropriate, to synthesize the control methodologies discussed in Refs. 10–12 with the POD-based reduced-order modeling methods studied in Ref. 4. In some sense, one could view this as the conventional approach. In fact, this line of research is being pursued by the authors. However, there are several inherent difficulties with such an approach. We briefly summarize some of these difficulties and discuss how the approach taken in this paper can be viewed as a complementary method addressing these challenges. First of all, we emphasize that, however positive the results in Ref. 4, this study considers an uncontrolled response regime. In fact, nearly all of the order reduction methodologies discussed above for nonlinear models of flow treat the uncontrolled system. A notable exception is presented in Refs. 9 and 13, which we discuss in some detail shortly. The difficulty, in the context of control, is not associated with producing a single reduced-order model that captures the essential dynamics of a particular operating or flow regime. This has been carried out quite successfully in Refs. 1–3, for example, or even in Ref. 4. Rather, if the overall goal of the model order reduction is to enable control of the system, the reduced-order model must be accurate over a diverse family of response regimes. In other words, because the express purpose of control is to alter, usually drastically, the system dynamics, any model derived from the response history of the open-loop, uncontrolled system may be a very poor approximation for the closed-loop system dynamics. This fact is well understood, and well documented, in the control theory and linear system theory literature (see, e.g., Ref. 6 and the references therein). Unfortunately, the problem is compounded in many applications to aeroelasticity or fluid mechanics in that the governing Navier–Stokes equations are inherently nonlinear. Some of the richest theory available for treating order reduction problems have been derived in the context of linear system theory. Researchers in structural dynamics and control have studied order reduction for decades as applied to structural systems. In some cases, surprisingly few Ritz basis vectors suffice for control. Thus, although a relatively small, fixed set of component modes (or Krylov vectors, attachment modes, constraint modes) may suffice to represent the dynamics of a structural system, empirical and anecdotal evidence suggests that this may not be the case for a large class of nonlinear fluid systems.

In this paper, we present a methodology that is directed precisely toward achieving efficient reduced-order representations of a class of nonlinear systems that is amenable to adaptive and online control methodologies. If we acknowledge that the underlying dynamics are, indeed, nonlinear a priori, a reasonable starting point is to choose one of the standard nonlinear system parameterizations. Possible choices include classical Fliess functional expansions, Chen series, or Volterra series. Silva has studied the identification of Volterra series from impulse response for aeroelastic applications.[14] We will consider the identification of similar systems, but for general input/output histories. Of course, Volterra series have been studied in numerous classical texts, such as those by Schetzen[15] and Rugh.[16] These methods have found an application in dynamical system modeling and control, even within the narrower context of aeroelastic systems. Still, it is likewise well known that Volterra series methods have not seen more widespread application as a result of their high dimensionality. Roughly speaking, a Volterra series is composed of a sum of integral operators, where each successive term in the sum is increasingly nonlinear. An approximation to the infinite sum is usually made by truncating the series after k terms. If the sampling interval is ΔT, the most naïve discretization of the continuous Volterra operators yield discrete Volterra operators expressed in terms of $\mathcal{O}(1/\Delta T^k)$ terms. The integer k is the number of integral operators retained in the sum. Attempts to achieve lower-order approximations have been made, most notably through the use of Laguerre orthogonal polynomials. This approach can be advantageous for some classes of stochastic inputs,[15] but it can still yield densely populated, high-order approximants for general inputs.

Because of these considerations, Nikolaou and Mantha[17] and Nikolaou and Vuthandam[18] have sought to exploit the specific properties of wavelets to overcome these difficulties. Wavelets and multiresolution analysis have gained notoriety for their applicability to image processing, signal and image compression, and denoising. They have likewise been used to advantage in the compression and approximation of integral operators.[19] It is important to note that the methodologies presented in Refs. 17 and 18, for example, make use of ad hoc wavelet basis selection and analogies to image compression to generate reduced-order Volterra models. These methodologies do not, however, derive from rigorous approximation (as in Ref. 19) of the integral operators comprising the Volterra series.

In the remainder of this paper, we derive order reduction methods for Volterra series by means of direct approximation of the constituent integral operators. In this sense, the paper uses the

philosophy given in Ref. 19, which focuses on second-kind Fredholm equations, in application to the multilinear Volterra integral operators. The result is a wavelet-based order reduction method, similar in intent to the multilevel methods discussed in Refs. 17 and 18. In Sec. II, we discuss the consistent approximation of Volterra series. The underlying biorthogonal wavelet approximation framework is discussed in Sec. III. Also discussed in Sec. III is the choice of biorthogonal wavelets that yields a consistent approximation of the constituent Volterra integral operators. Finally, Sec. IV presents numerical results and validation studies.

II. Volterra Operators and Approximation

We will consider those dynamical systems expressed in terms of Volterra integral operators, and we restrict our attention to single-input/single-output systems. The output $y(t)$ can be written formally as the infinite sum

$$y(t) = y_1(t) + y_2(t) + y_3(t) + y_4(t) + \cdots \tag{1}$$

where each term $y_i(t)$ is the output of the ith-order Volterra integral operator. For $i = 1$ or 2, we have

$$y_1(t) = \int_{-\infty}^{t} h_1(t-\xi)u(\xi)\,\mathrm{d}\xi \tag{2}$$

$$y_2(t) = \int_{-\infty}^{t}\int_{-\infty}^{t} h_2(t-\xi, t-\eta)u(\xi)u(\eta)\,\mathrm{d}\xi\,\mathrm{d}\eta \tag{3}$$

where $u(\xi)$ and $u(\eta)$ represent the system inputs and $h_1(t-\xi)$, $h_2(t-\xi, t-\eta)$ represent the first- and second-order Volterra kernels, respectively. The theoretical foundations of the Volterra series in Eq. (1), sufficient conditions for its convergence, and the form for higher-order terms can be found in Ref. 15. In this paper, we are concerned only with the first- and second-order ($i = 1$ and 2) terms of the Volterra series. With the use of a simple change of variables, it can be shown that the first- and second-order Volterra operators can be written in the form[20]

$$y_1(t) = \int_{0}^{+\infty} h_1(\xi)u(t-\xi)\,\mathrm{d}\xi \tag{4}$$

$$y_2(t) = \int_{0}^{\infty}\int_{0}^{\infty} h_2(\xi, \eta)u(t-\xi)u(t-\eta)\,\mathrm{d}\xi\,\mathrm{d}\eta \tag{5}$$

where the operators are defined over semi-infinite domains.

Now, we introduce the characteristic function $\chi(t)$ of the unit interval $[0, 1]$,

$$\chi(t) = \begin{cases} 1, & t \in [0, 1] \\ 0, & \text{otherwise} \end{cases} \tag{6}$$

and its scaled and dilated translates

$$\begin{aligned} \chi_{j,k}(t) &= 2^{j/2}\chi(2^j t - k) \\ &= \begin{cases} 2^{j/2}, & 2^j t - k \in [0, 1] \\ 0, & \text{otherwise} \end{cases} \\ &= \begin{cases} 2^{j/2}, & k2^{-j} \le t \le (k+1)2^{-j} \\ 0, & \text{otherwise} \end{cases} \end{aligned} \tag{7}$$

Note carefully that the integer j defines the sampling step to be 2^{-j}. We can obtain a zero-order hold approximation of the input by writing

$$u(t) = \sum_{k=0}^{\infty} u_{j,k}\chi_{j,k}(t) \tag{8}$$

After some tedious algebra, it is shown in Ref. 20 that the zero-order hold approximation of both the first- and second-order operators of the Volterra series is simply

$$y_{j,n} = \sum_{m=n-1}^{0} h_{1,j,m}u_{j,n-m-1} + \sum_{r,s=n-1}^{0} h_{2,j,(r,s)}u_{j,n-r-1}u_{j,n-s-1} \tag{9}$$

where the discrete first- and second-order Volterra kernels are defined as

$$h_{1,j,m} = 2^{j/2}\int_{m2^{-j}}^{(m+1)2^{-j}} h_1(\xi)\,\mathrm{d}\xi, \qquad \text{for} \qquad m \ge 0 \tag{10}$$

$$h_{2,j,(r,s)} = 2^{j/2}2^{j/2}\int_{r2^{-j}}^{(r+1)2^{-j}}\int_{s2^{-j}}^{(s+1)2^{-j}} h_2(\xi, \eta)\,\mathrm{d}\xi\,\mathrm{d}\eta \qquad \text{for} \qquad r, s \ge 0 \tag{11}$$

Thus far, we have shown that the zero-order hold for both the input and output induces the discrete Volterra Series in Eq. (9). We now show that the discrete integrals in Eqs. (10) and (11) are amenable to wavelet-induced multilevel approximation. Suppose that the first-order kernel $h_1(\xi)$ is approximated as

$$h_1(\xi) = \sum_{p} h_{1,j,p}\phi_{j,p}(\xi) \tag{12}$$

where the only assumption on the functions $\phi_{j,p}(\xi)$ at this point is that they are dual to $\chi_{j,k}(\xi)$ in the sense that

$$\int_{R} \phi_{j,p}(\xi)\chi_{j,k}(\xi) = \delta_{p,k} \tag{13}$$

The discrete output of the first-order Volterra operator in Eq. (5) becomes

$$\begin{aligned} y_{1,j,n} &= \sum_{m=0}^{\infty}\int_{0}^{\infty}\sum_{p} h_{1,j,p}\phi_{j,p}(\xi)\chi_{j,n-m-1}(\xi)\,\mathrm{d}\xi u_{j,m} \\ y_{1,j,n} &= \sum_{m,p} h_{1,j,p}\int_{0}^{\infty}\phi_{j,p}(\xi)\chi_{j,n-m-1}(\xi)\,\mathrm{d}\xi u_{j,m} \end{aligned} \tag{14}$$

which can be rewritten as

$$y_{1,j,n} = \sum_{m} h_{1,j,n-m-1}u_{j,m} \tag{15}$$

or, letting $s = n - m - 1$,

$$y_{1,j,n} = \sum_{s} h_{1,j,s}u_{j,n-s-1} \tag{16}$$

The details of the derivation of the form of the discrete first-order Volterra operator shown in Eq. (16) can be found in Ref. 20. Likewise, if we approximate the second-order kernel as

$$\begin{aligned} h_2(\xi, \eta) &= \sum_{r,s} h_{2,j,(r,s)}\Phi_{j,(r,s)}(\xi, \eta) \\ &= \sum_{r}\sum_{s} h_{2,j,(r,s)}\phi_{j,r}(\xi)\phi_{j,s}(\eta) \end{aligned} \tag{17}$$

and substitute this kernel in Eq. (6), we recover, for the discrete output of the second-order Volterra operator,

$$\begin{aligned} y_{2,j,n} &= \sum_{k,m=0}^{\infty}\int_{0}^{\infty}\int_{0}^{\infty}\sum_{r,s} h_{2,j,(r,s)}\phi_{j,r}(\xi)\phi_{j,s}(\eta)\chi_{j,n-k-1}(\xi) \\ &\quad \times \chi_{j,n-m-1}(\eta)\,\mathrm{d}\xi\,\mathrm{d}\eta\, u_{j,k}u_{j,m} \\ y_{2,j,n} &= \sum_{k,m,r,s} h_{2,j,(r,s)}\delta_{(r,s),(n-k-1,n-m-1)}u_{j,k}u_{j,m} \\ y_{2,j,n} &= \sum_{k,m} h_{2,j,(n-k-1,n-m-1)}u_{j,k}u_{j,m} \end{aligned} \tag{18}$$

Letting $r = n - k - 1$ and $s = n - m - 1$, we obtain

$$y_{2,j,n} = \sum_{r,s} h_{2,j,(r,s)}u_{j,n-r-1}u_{j,n-s-1} \tag{19}$$

The details of the derivation of the form of the discrete second-order Volterra operator shown in Eq. (19) can be found in Ref. 20. Indeed,

Eqs. (16) and (19) illustrate that, as long as the approximating family is biorthogonal with respect to the characteristic functions $\chi_{j,k}$, we obtain the discrete input and output Volterra Series derived in Eq. (9) by a zero-order hold of the input and output. In the next section, we discuss the specific selection of a biorthogonal wavelet basis to achieve the desired approximation and order reduction.

III. Biorthogonal Wavelet Approximations

In Sec. II, we showed that a consistent approximation of the discrete Volterra input/output mapping is achieved when kernel approximants are selected to be biorthogonal with respect to characteristic functions of dyadic intervals. In this section we discuss a class of biorthogonal wavelets that satisfy this condition and induce a multilevel approximation of the Volterra kernels. Recall that a multiresolution analysis is a nested sequence of spaces $\{V_k\}_{k\in Z}$

$$\cdots V_{-1} \subset V_0 \subset V_1 \subset V_2 \cdots \tag{20}$$

where V_0 is the span of the translates of a fixed function $\phi(x)$:

$$V_0 = \operatorname*{span}_{k\in Z}\{\phi(x-k)\} \tag{21}$$

In this equation, Z is the collection of (signed) integers. The remaining spaces in the sequence of Eq. (20) are defined by dilation. We define

$$\phi_{j,k}(x) = 2^{j/2}\phi(2^j x - k) \tag{22}$$

and, subsequently,

$$V_j = \operatorname*{span}_{k\in Z}\{\phi_{j,k}(x)\} \tag{23}$$

If we have a second multiresolution $\{\tilde{V}_k\}_{k\in Z}$ generated by the function $\tilde{\phi}(x)$, we say that the pair $\{V_k\}_{k\in Z}$ and $\{\tilde{V}_k\}_{k\in Z}$ form a biorthogonal multiresolution provided that

$$\langle \phi_{j,k}(x), \tilde{\phi}_{j,m}(x)\rangle = \int_R \phi_{j,k}(x)\tilde{\phi}_{j,m}(x)\,\mathrm{d}x = \delta_{k,m} \tag{24}$$

A wavelet $\psi(x)$ is a function whose dilates and translates span the complement spaces W_j defined by

$$V_{j+1} = V_j \oplus W_j \tag{25}$$

so that

$$W_j = \operatorname*{span}_{k\in Z}\{\psi_{j,k}(x)\} \tag{26}$$

where

$$\psi_{j,k}(x) = 2^{j/2}\psi(2^j x - k) \tag{27}$$

A similar definition holds for the dual wavelet $\tilde{\psi}(x)$. As discussed in Ref. 21, it is possible to define dual wavelets $\psi(x)$ and $\tilde{\psi}(x)$ associated with the biorthogonal multiresolution analyses $\{V_k\}_{k\in Z}$ and $\{\tilde{V}_k\}_{k\in Z}$ that satisfy

$$\langle \psi_{j,k}(x), \tilde{\psi}_{m,n}(x)\rangle = \delta_{(j,k),(m,n)} \tag{28}$$

In particular, this can hold if we find masks $\{a_k\}$, $\{b_k\}$, $\{\tilde{a}_k\}$, and $\{\tilde{b}_k\}$ that satisfy the two-scale relationships:

$$\begin{aligned} \phi(x) &= \sqrt{2}\sum_k a_k\phi(2x-k), \qquad & \tilde{\phi}(x) &= \sqrt{2}\sum_k \tilde{a}_k\tilde{\phi}(2x-k) \\ \psi(x) &= \sqrt{2}\sum_k b_k\phi(2x-k), \qquad & \tilde{\psi}(x) &= \sqrt{2}\sum_k \tilde{b}_k\tilde{\phi}(2x-k) \end{aligned} \tag{29}$$

where

$$b_k = (-1)^k\tilde{a}_{-k+1}, \qquad \tilde{b}_k = (-1)^k a_{-k+1} \tag{30}$$

If Eqs. (29) and (30) are satisfied, fast multilevel algorithms can be derived that project a function onto various nested spaces. If $f(\xi) \in V_j$, then $f(\xi)$ has a representation

$$f(\xi) = \sum_k \alpha_{j,k}\phi_{j,k}(\xi) \tag{31}$$

by means of Eq. (23), where the $\{\alpha_{j,k}\}$ are constant scaling function coefficients. An equivalent expansion of $f(\xi)$ can be written by means of Eq. (25) as

$$f(\xi) = \sum_k \alpha_{j-1,k}\phi_{j-1,k}(\xi) + \sum_k \beta_{j-1,k}\psi_{j-1,k}(\xi) \tag{32}$$

where the $\{\alpha_{j-1,k}\}$ and $\{\beta_{j-1,k}\}$ are constant scaling function and wavelet coefficients, respectively. Given the finer-scale coefficients $\{\alpha_{j,k}\}$ in Eq. (31), it is straightforward to derive the following decomposition formulas by which we can calculate the coarser-scale coefficients $\{\alpha_{j-1,k}\}$ and $\{\beta_{j-1,k}\}$ in Eq. (32):

$$\alpha_{j-1,k} = \sum_n \tilde{a}_{n-2k}\alpha_{j,n} \tag{33}$$

$$\beta_{j-1,k} = \sum_n \tilde{\beta}_{n-2k}\alpha_{j,n} \tag{34}$$

As an example, we obtain

$$\langle f(\xi), \tilde{\phi}_{j-1,m}(\xi)\rangle = \alpha_{j-1,m} = \sum_k \alpha_{j,k}\langle \phi_{j,k}(\xi), \tilde{\phi}_{j-1,m}(\xi)\rangle \tag{35}$$

Making use of the two-scale equation and biorthogonality properties of the scaling functions, we have

$$\begin{aligned} \alpha_{j-1,m} &= \sum_k \alpha_{j,k}\left\langle \phi_{j,k}(\xi), \sum_s \tilde{a}_s\tilde{\phi}_{j,2m+s}(\xi)\right\rangle \\ &= \sum_{k,s} \alpha_{j,k}\tilde{a}_s\delta_{k,2m+s} \\ &= \sum_k \tilde{a}_{k-2m}\alpha_{j,k} \end{aligned} \tag{36}$$

Equations (33) and (34) are the decomposition formulas associated with the set of biorthogonal wavelets (ϕ, ψ) and $(\tilde{\phi}, \tilde{\psi})$. A reconstruction formula can likewise be derived that gives the finer-scale coefficients in terms of the coarser-scale coefficients:

$$\alpha_{j,m} = \sum_k (a_{m-2k}\alpha_{j-1,k} + b_{m-2k}\beta_{j-1,k}) \tag{37}$$

These expressions can be used to obtain a multilevel representation of the Volterra kernels. Assume that the first-order Volterra kernel is expressed on the finest scale as

$$h_1(\xi) = \sum_p h_{1,j,p}\phi_{j,p}(\xi) = \sum_p \alpha_{j,p}\phi_{j,p}(\xi) \tag{38}$$

where

$$\begin{aligned} h_{1,j,p} = \alpha_{j,p} &= \int_0^\infty h_1(\xi)\chi_{j,p}(\xi)\,\mathrm{d}\xi \\ &= \int_{p2^{-j}}^{(p+1)2^{-j}} h_1(\xi)\,\mathrm{d}\xi, \qquad \text{for} \qquad p \geq 0 \end{aligned} \tag{39}$$

That is, we have identified $\chi_{j,p}(\xi) \equiv \tilde{\phi}_{j,p}(\xi)$. With a recursive application of Eq. (25), a multilevel expansion of the first-order kernel is obtained:

$$\begin{aligned} h_1(\xi) = \sum_p \alpha_{j_0,p}\phi_{j_0,p}(\xi) &+ \sum_p \beta_{j_0,p}\psi_{j_0,p}(\xi) && \text{(level } j_0\text{)} \\ &+ \sum_p \beta_{j_1,p}\psi_{j_1,p}(\xi) && \text{(level } j_1\text{)} \\ &+ \sum_p \beta_{j_2,p}\psi_{j_2,p}(\xi) && \text{(level } j_2\text{)} \\ &\vdots \\ &+ \sum_p \beta_{j-1,p}\psi_{j-1,p}(\xi) && \text{(level } j-1\text{)} \end{aligned}$$

$$h_1(\xi) = \sum_p \alpha_{j_0,p}\phi_{j_0,p}(\xi) + \sum_{l=j_0}^{j-1}\sum_p \beta_{l,p}\psi_{l,p}(\xi) \tag{40}$$

Similarly, if we define the tensor product scaling functions

$$\Phi(\xi,\eta)=\phi(\xi)\phi(\eta),\qquad \tilde{\Phi}(\xi,\eta)=\tilde{\phi}(\xi)\tilde{\phi}(\eta) \tag{41}$$

and the tensor product wavelets

$$\begin{aligned}
\Psi^1(\xi,\eta)&=\phi(\xi)\psi(\eta), & \tilde{\Psi}^1(\xi,\eta)&=\tilde{\phi}(\xi)\tilde{\psi}(\eta)\\
\Psi^2(\xi,\eta)&=\psi(\xi)\phi(\eta), & \tilde{\Psi}^2(\xi,\eta)&=\tilde{\psi}(\xi)\tilde{\phi}(\eta)\\
\Psi^3(\xi,\eta)&=\psi(\xi)\psi(\eta), & \tilde{\Psi}^3(\xi,\eta)&=\tilde{\psi}(\xi)\tilde{\psi}(\eta)
\end{aligned} \tag{42}$$

we obtain the following single-scale representation of the second-order kernel:

$$h_2(\xi,\eta)=\sum_{r,s}\alpha_{j,(r,s)}\Phi_{j,(r,s)}(\xi,\eta) \tag{43}$$

The corresponding two-scale expansion of the kernel is

$$\begin{aligned}
h_2(\xi,\eta)&=\sum_{r,s}\alpha_{j-1,(r,s)}\Phi_{j-1,(r,s)}(\xi,\eta)\\
&+\sum_{r,s}\beta^1_{j-1,(r,s)}\Psi^1_{j-1,(r,s)}(\xi,\eta)+\sum_{r,s}\beta^2_{j-1,(r,s)}\Psi^2_{j-1,(r,s)}(\xi,\eta)\\
&+\sum_{r,s}\beta^3_{j-1,(r,s)}\Psi^3_{j-1,(r,s)}(\xi,\eta)
\end{aligned} \tag{44}$$

The identification of reduced-order representations of the discrete first- and second-order Volterra kernels is, of course, dependent on the multilevel structure induced by our choice of a biorthogonal wavelet basis. Recall that the discrete first-order Volterra operator has the form

$$y_{1,j,n}=\sum_s h_{1,j,s}u_{j,n-s-1}=\sum_s \alpha_{j,s}u_{j,n-s-1} \tag{45}$$

where the $\{\alpha_{j,s}\}$ are the scaling function coefficients in the single-scale representation of the first-order Volterra kernel shown in Eq. (38). Equation (45) can be written in matrix form as

$$\boldsymbol{y}_j=[U]\,\boldsymbol{\alpha}_j \tag{46}$$

where $\boldsymbol{y}_j$ is a vector of discrete outputs, $\boldsymbol{\alpha}_j$ is a vector of scaling function coefficients, and $[U]$ is a lower triangular matrix composed of discrete inputs:

$$[U]=\begin{bmatrix}
u_0 & 0 & 0 & \cdots & 0\\
u_1 & u_0 & 0 & \cdots & 0\\
u_2 & u_1 & u_0 & \cdots & 0\\
u_3 & u_2 & u_1 & \ddots & \vdots\\
\vdots & \vdots & \vdots & \cdots & u_0
\end{bmatrix} \tag{47}$$

Recall from Eq. (40) that our choice of a wavelet basis affords a multiscale expansion of the first-order kernel. Let us define $\boldsymbol{\beta}$ as the multiscale vector of coefficients:

$$\boldsymbol{\beta}\triangleq\begin{Bmatrix}
\boldsymbol{\alpha}_{j_0}\\
\boldsymbol{\beta}_{j_0}\\
\boldsymbol{\beta}_{j_1}\\
\vdots\\
\boldsymbol{\beta}_{j-1}
\end{Bmatrix} \tag{48}$$

where j_0 is the coarsest level chosen in the multiscale representation. In Ref. 20, it is demonstrated that, through a recursive application of the decomposition formulas shown in Eqs. (33) and (34), an invertible matrix $[T]$ can be constructed that transforms the single-scale vector of coefficients into the multiscale vector:

$$\boldsymbol{\beta}=[T]\,\boldsymbol{\alpha}_j,\qquad \boldsymbol{\alpha}_j=[T]^{-1}\boldsymbol{\beta} \tag{49}$$

It should be noted that the matrix $[T]$ is rarely constructed in practice, but rather the decomposition equations are applied explicitly. Equation (46) can now be written as

$$\boldsymbol{y}_j=[U][T]^{-1}\boldsymbol{\beta} \tag{50}$$

So far, no order reduction has taken place and $\boldsymbol{\beta}$ has the same cardinality as $\boldsymbol{y}_j$. At this point, order reduction is achieved by truncating $\boldsymbol{\beta}$, keeping only the coefficients from the coarsest levels, and setting the rest of the coefficients to zero. The nonzero terms in $\boldsymbol{\beta}$ are then found that minimize the least-square error between the actual output and the identified output.

To obtain a reduced-order representation of the second-order Volterra kernel, recall that the output of the discrete second-order Volterra operator takes the form

$$\begin{aligned}
y_{2,j,n}&=\sum_{r,s}h_{2,j,(r,s)}u_{j,n-r-1}u_{j,n-s-1}\\
&=\sum_{r,s}\alpha_{j,(r,s)}u_{j,n-r-1}u_{j,n-s-1}
\end{aligned} \tag{51}$$

where the $\{\alpha_{j,(r,s)}\}$ represent the coefficients in the single-scale expansion of the second-order kernel shown in Eq. (43). Just as in the one-dimensional case, there is an equivalent multiscale expansion of the second-order kernel. In this representation, we have a two-dimensional array of multiscale coefficients having the structure

$$[\beta]=\left[\begin{array}{cccc|c}
[\alpha_{j_0}] & [\beta^1_{j_0}] & \cdots & | & \\
[\beta^2_{j_0}] & [\beta^3_{j_0}] & \cdots & | & [\beta^1_{j-1}]\\
\vdots & \vdots & \ddots & | & \\
\hline
 & [\beta^2_{j-1}] & & | & [\beta^3_{j-1}]
\end{array}\right] \tag{52}$$

where j_0 is the coarsest level in the expansion. In Eq. (52), $[\alpha_{j_0}]$ represents the two-dimensional array of scaling function coefficients at level j_0; $[\beta^1_{j_0}]$, $[\beta^2_{j_0}]$, and $[\beta^3_{j_0}]$ represent the two-dimensional arrays of wavelet coefficients at level j_0; and so forth. At this point, just as in the one-dimensional case, order reduction is achieved by truncating $[\beta]$, keeping only the coarser-scale coefficients, and setting the rest equal to zero. Then, to obtain a reduced-order identification of the output of a nonlinear system by using the first- and second-order Volterra operators, the nonzero coefficients in $\boldsymbol{\beta}$ (from the first-order operator) and $[\beta]$ (from the second-order operator) are found that minimize the least-square error between the actual output and the identified output.

IV. Numerical and Experimental Results

In a series of papers,[10–12] we have derived, implemented, and tested reduced-order models for the prototypical nonlinear aeroelastic system depicted in Fig. 1. This system is composed of a NACA0012 airfoil that is capable of undergoing large amplitude response in either the pitch or plunge degrees of freedom. Any reasonable representation of the response of this system is inherently geometrically nonlinear, as a result of the unique design of the carriage on which the airfoil is mounted. The details of the design, shown schematically in Fig. 2, are described in detail in Refs. 10–12. This system has been designed to exhibit large amplitude limit cycle oscillations in particular flow regimes, and the performance of geometrically nonlinear closed-loop control methods is discussed in Refs. 10–12. We note that a conventional representation of the nonlinear dynamics of this system that was used in these previous

studies comprised two parametrically dependent, coupled nonlinear ordinary differential equations of second order. This is, perhaps, the simplest nonlinear model that could be used to represent the system. The pitch amplitude is so large that it may also be argued that stall effects likewise contribute significant nonlinear response that is not accounted for in the open-loop model used in Refs. 10–12. In any event, in the current numerical example, we study the performance of the wavelet-based Volterra series system identification for this example. Angle encoders provide a measurement of the flap deflection as a function of time, which we take as input to the wavelet-based kernel identification algorithm. We choose the output to be the pitch angle, also measured by angle encoders as depicted in Fig. 1, measured in radians. In this simple numerical experiment, we consider the experimental records from a single test. The measured flap deflection, measured pitch angle, and flow velocity in the tunnel are depicted in Figs. 3–5, respectively. The entire data set is composed of 2048 sample points. With the use of a sliding window of 128 sample points, a weakly nonlinear Volterra series representation composed of only the first- and second-order kernels was identified for the system. For this specific numerical test, within each sample window, the first-order kernel was composed of four terms, whereas the second-order kernel was composed of a 4×4 array. It should be noted that the 4×4 array is symmetric (see Schetzen[15]), so that the cardinality of the Volterra series model is $4 + (5 \times \frac{4}{2}) = 14$ terms. The difference between the experimental output and the output of the identified model is depicted in Fig. 6.

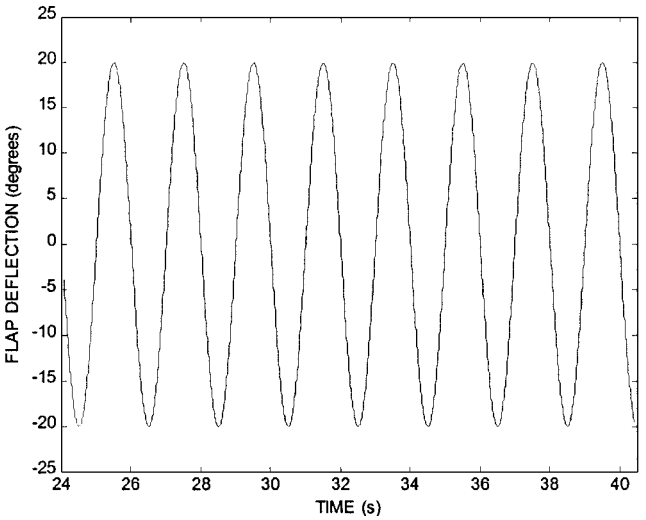

Fig. 3 Experimental input: flap deflection.

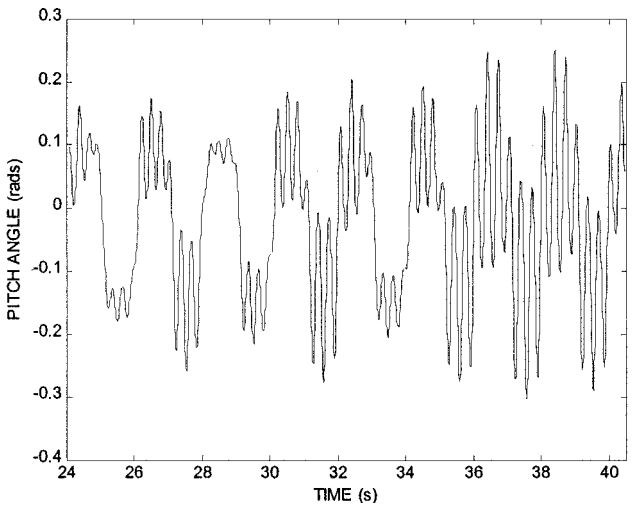

Fig. 4 Experimental output: pitch angle.

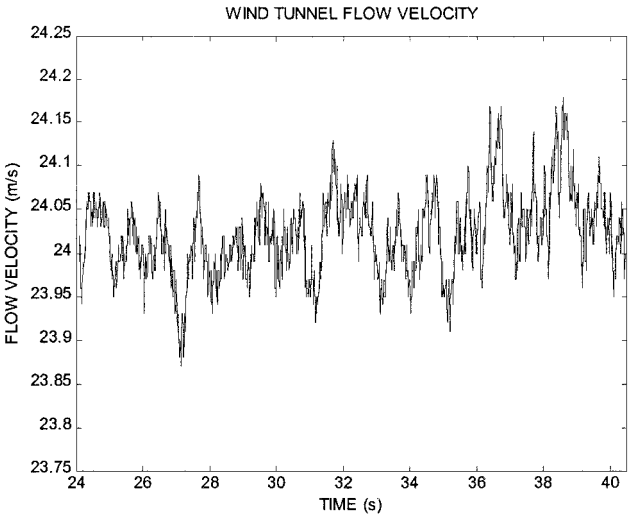

Fig. 5 Flow velocity in the test section.

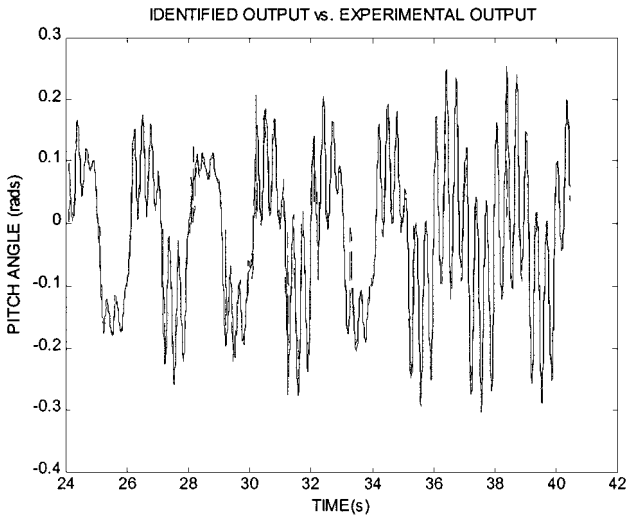

Fig. 6 Predicted output from model identification (– – –) and experimental output (——).

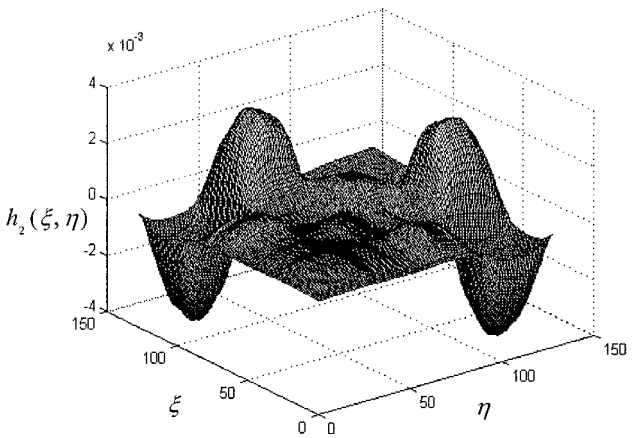

Fig. 7 Identified second-order Volterra kernel from the first sample window.

From the figure, the identified output (represented by the dashed line) is barely discernible from the actual experimental output (represented by the solid line). Finally, the evolution of the kernels that comprise this system is depicted in Figs. 7–10. Figures 7–10 show the second-order Volterra kernels associated with the first, second, third, and fourth sample windows, respectively. Each second-order kernel is represented in terms of the same ten basis functions. It is clear from the figures that the second-order kernels evolve in time for this system.

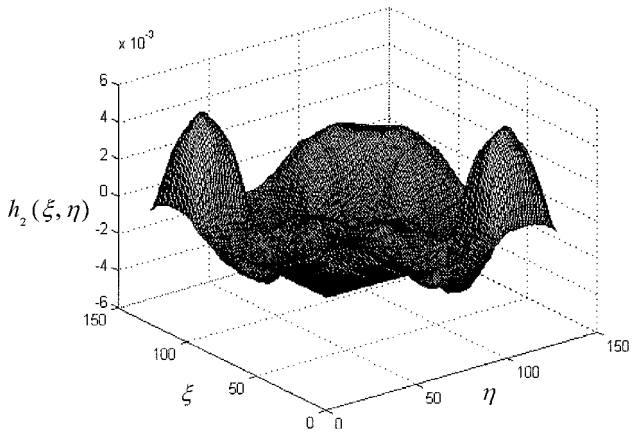

Fig. 8 Identified second-order Volterra kernel from the second sample window.

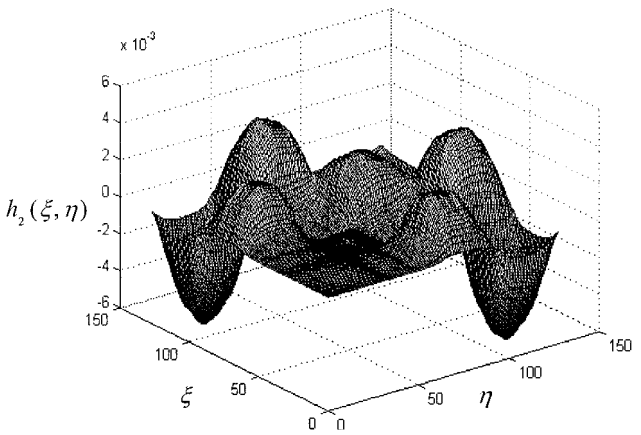

Fig. 9 Identified second-order Volterra kernel from the third sample window.

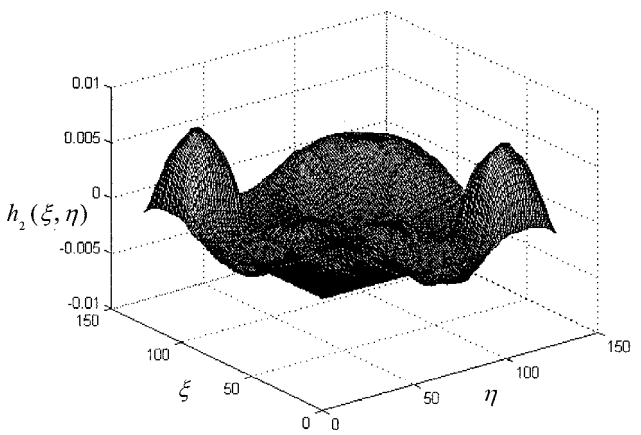

Fig. 10 Identified second-order Volterra kernel from the fourth sample window.

V. Conclusions

This paper has derived a wavelet- and multiresolution-based methodology for obtaining reduced-order approximations of Volterra series. Although Volterra series representations provide a succinct characterization of nonlinear system response in principle, their use has been limited in practice because of the large number of terms required to represent the higher order, nonlinear terms. We show that a consistent approximation of the Volterra input/output representation is achieved if two conditions are satisfied: 1) a zero-order hold is used for the input and output sequences; 2) a biorthogonal wavelet family is selected such that the generator is dual to characteristic functions that define the zero-order hold.

The identification of a prototypical nonlinear aeroelastic system is studied to evaluate the potential of the derived method. The prototypical aeroelastic system undergoes large amplitude, limit cycle oscillations. Nevertheless, the wavelet identification of the nonlinear response was extremely accurate with the reduced-order wavelet models. For a sample record size of 2048 data points and a sliding window of 128 data points, the nonlinear response character within each sample window was captured with as few as 14 wavelets. It was also shown that the nonlinear second-order kernel did evolve in time. However, this evolution was essentially slowly varying. One implication of the numerical tests is that the migration of these methodologies to on-line identification of Volterra kernels should be investigated immediately.

This paper suggests several subsequent lines of research. Although the ability of the wavelet representations to compress integral operators was exploited implicitly, the methodology does not currently make use of the explicit multilevel structure that is available. For example, it is anticipated that multilevel and multigrid methods can be used to improve the convergence rate of the identification procedure. Essentially, the method would perform multiscale filtering of the input and output sequences a priori, before the kernels of the nonlinear system are estimated. The kernels themselves could then be estimated based on resolutions that correspond to the filtered input and output sequences. Additionally, this paper also suggests that there should be a careful study of energy exchange in time-scale space for classical nonlinear dynamical systems of aeroelasticity. The structure of the kernels may be indicative of the time-frequency evolution of energy in the system. Finally, the identification procedure suggested in this paper is most useful when we can derive associated compensators for the nonlinear Volterra series. Such work has been studied in some classical texts, but the specific forms of the desired compensators for the multiresolution kernels have not been studied.

References

[1]Reichert, R. S., Hatay, F. F., Biringen, S., and Huser, A., "Proper Orthogonal Decomposition Applied to Turbulent Flow in a Square Duct," *Journal of Physics of Fluids*, Vol. 6, No. 9, 1994, pp. 3086–3092.

[2]Tang, K. Y., Graham, W. R., and Peraire, J., "Active Flow Control Using a Reduced Order Model and Optimum Control," AIAA Paper 96-1946, June 1996.

[3]Ly, H. V., and Tran, H. T., "Proper Orthogonal Decomposition for Flow Calculations and Optimal Control in a Horizontal CVD Reactor," TR, Center for Research in Scientific Computation, North Carolina State Univ., Raleigh, NC, 1997.

[4]Rediniotis, O., and Kurdila, A. J., "Reduced Order Navier–Stokes Models for Synthetic Jets," *Proceedings of DETC'99: The ASME 1999 Design Engineering Technical Conference*, American Society of Mechanical Engineers, Fairfield, NJ, 1999.

[5]Craig, R. R., *Structural Dynamics, An Introduction to Computer Methods*, J. Wiley, New York, 1981, pp. 467–496.

[6]Skelton, R. E., *Dynamic Systems Control, Linear Systems Analysis and Synthesis*, Wiley, New York, 1988, pp. 266–293.

[7]Aubry, N., Holmes, P., Lumley, J. L., and Stone, E., "The Dynamics of Coherent Structures in the Wall Region of a Turbulent Boundary Layer," *Journal of Fluid Mechanics*, Vol. 192, 1988, pp. 115–173.

[8]Ball, K. S., Sirovich, L., and Keefe, L. R., "Dynamical Eigenfunction Decomposition of Turbulent Channel Flow," *International Journal for Numerical Methods in Fluids*, Vol. 12, No. 6, 1991, pp. 585–604.

[9]Ito, K., and Ravindran, S. S., "Reduced Basis Method for Flow Control," TR, Center for Research in Scientific Computation, North Carolina State Univ., Raleigh, NC, 1997.

[10]Ko, J., Strganac, T. W., and Kurdila, A. J., "Stability and Control of a Structurally Nonlinear Aeroelastic System," *Journal of Guidance, Control, and Dynamics*, Vol. 21, No. 5, 1998, pp. 718–725.

[11]Ko. J., Strganac, T. W., and Kurdila, A. J., "Adaptive Feedback Linearization for the Control of a Typical Wing Section with Structural Nonlinearity," *Nonlinear Dynamics*, Vol. 18, No. 3, 1999, pp. 289–301.

[12]Ko, J., Kurdila, A. J., and Strganac, T. W., "Nonlinear Control of a Prototypical Wing Section with Torsional Nonlinearity," *Journal of Guidance, Control, and Dynamics*, Vol. 20, No. 6, 1997, pp. 1181–1189.

[13]Ito, K., and Ravindran, S. S., "A Reduced Basis Method for Control Problems Governed by PDEs," TR, Center for Research in Scientific Computation, North Carolina State Univ., Raleigh, NC, 1997.

[14]Silva, W. A., "Discrete-Time Linear and Nonlinear Aerodynamic

Impulse Responses for Efficient CFD Analyses," Ph.D. Dissertation, College of William and Mary, Williamsburg, VA, 1997.

[15]Schetzen, M., *The Volterra and Wiener Theories of Nonlinear Systems*, Wiley, New York, 1980, pp. 1–208.

[16]Rugh, W. J., *Nonlinear System Theory, The Volterra-Wiener Approach*, Johns Hopkins Univ. Press, Baltimore, MD, 1981, pp. 1–268.

[17]Nikolaou, M., and Mantha, D., "Efficient Nonlinear Modeling Using Wavelets and Related Compression Techniques," *NSF Workshop on Nonlinear Model Predictive Control*, Ascona, Switzerland, 1998.

[18]Nikolaou, M., and Vuthandam, P., "FIR Model Identification: Parsimony Through Kernel Compression with Wavelets," *AIChE Journal*, Vol. 44, No. 1, 1998, pp. 141–150.

[19]Chen, Z., Micchelli, C. A., and Xu, Y., "The Petrov-Galerkin Method for Second Kind Integral Equations II: Multiwavelet Schemes," *Advances in Computational Mathematics*, Vol. 7, No. 3, 1997, pp. 199–233.

[20]Prazenica, R. J., "Wavelets and Reduced Order Modeling of Dynamical Systems," M.S. Thesis, Univ. of Florida, Gainesville, FL, 1999.

[21]Cohen, A., Daubechies, I., and Feauveau, J. C., "Biorthogonal Bases of Compactly Supported Wavelets," *Communications on Pure and Applied Mathematics*, Vol. 45, 1992, pp. 485–560.